J. Fluid Mech. (1985), vol. 159, pp. 131–150
Printed in Great Britain

On the evidence for the effect of bubble interference on cavitation noise

By VIJAY H. ARAKERI AND V. SHANMUGANATHAN
Indian Institute of Science, Bangalore, 560 012, India

(Received 22 January 1985)

Cavitation-noise measurements from an axisymmetric body with 'controlled' generation of cavitation are reported. The control was achieved by seeding artificial nuclei in the boundary layer by electrolysis. It was possible to alter the number density of nuclei by varying the electrolysis voltage, polarity and the geometry of the electrode. From the observed trend of cavitation-noise data it is postulated that there exists an 'interference effect' which influences cavitation noise. When the nucleus-number density is high and cavitation numbers are low this effect is strong. Under these conditions the properties of cavitation noise are found to differ considerably from those expected based on theories concerning noise from single-spherical-bubble cavitation.

1. Introduction

The type of cavitation observed on a solid body depends primarily on two factors; namely the availability of 'nuclei', which are the weak spots in the liquid sample, and the viscous-flow characteristics of the body. Excellent sources of nuclei are undissolved air bubbles, typically of 50 μm in size, and when these are available in sufficient numbers then the type of cavitation commonly observed is 'travelling-bubble cavitation'. Physically this consists of the growth of nuclei into macroscopic cavities as they are brought by the flow into the low-pressure regions and their subsequent collapse. The dynamics of such cavitation bubbles was photographed by Knapp & Hollander (1948) and analysed by Plesset (1949) by extending the original formulation of Rayleigh (1917) for the dynamics of a single spherical cavitation bubble. The history of a typical cavitation bubble observed by Knapp & Hollander was predicted quite accurately by Plesset; however, a natural question would be whether the consideration of single-bubble dynamics would be sufficient when the distance between neighbouring bubbles in a cavitation zone is so small that individual bubbles interact with each other. This point has received very little attention in cavitation research, perhaps because there is no direct experimental evidence to suggest clearly that the dynamics of a cavitation bubble are influenced by the presence of neighbouring bubbles. The primary aim of the present work is to provide this evidence by studying one of the physical effects owing to cavitation-bubble dynamics, namely the radiated noise which is termed 'cavitation noise'. This was achieved by measuring cavitation noise from an axisymmetric body on which controlled cavitation of the travelling-bubble type was generated by seeding artificial nuclei in the boundary layer by electrolysis.

In §2 the experimental methods and the instrumentation used are described. In §3 the cavitation-inception characteristics of the body with and without seeding of artificial nuclei are discussed. Typical results indicating the influence of various

parameters, such as velocity, on cavitation noise are presented in §4. In §5 the results are presented in non-dimensional form with non-dimensionalization based on the approach suggested by Blake, Wolpert & Geib (1977) and using single-bubble-dynamics parameters. From the results of non-dimensionalization certain obvious trends are noted which clearly give evidence for the interference effect; this point is highlighted in §6, followed by a discussion in §7, and finally a summary is provided in §8.

2. Experimental methods

2.1. *Test body and facility*

As indicated, one of the primary objectives of the present study was to measure cavitation noise from a well-defined type of cavitation, namely the travelling-bubble type. It was expected that this could be achieved by seeding the flow with artificial nuclei generated by electrolysis. In order to exploit fully this technique it was necessary to choose the test body carefully to avoid any influence on cavitation from other extraneous parameters. Previous findings (Arakeri & Acosta 1973; and Blake *et al.* 1977) have indicated that one such important parameter is the presence of laminar separation. Thus one of the requirements for the present test body was that there should not be laminar separation at the test Reynolds numbers, the range being 10^5–10^6. Among the several axisymmetric bodies used for cavitation studies an axisymmetric headform commonly known as a 'Schiebe nose' seemed to satisfy this requirement (Vander Muelen 1976; Gates 1979). The contour of this body is generated by the potential-flow solution to a distributed source disk oriented normally to a uniform flow, and it was first introduced for cavitation studies by Schiebe (1972). In the present case the shape with the minimum pressure coefficient $C_{p\,\min}$ of -0.75 was selected. The geometrical shape and the theoretical pressure distribution for this body, taken from Gates *et al.* (1979), is shown in figure 1. The nose portion of the body was made from a Perspex rod, for reasons to be indicated later, and this was attached to a cylindrical stainless-steel afterbody of diameter 50 mm. The combined test body was mounted securely with a three-bladed sting support in the 381 mm closed jet test section of the Indian Institute of Science high-speed water-tunnel facility. A schematic of the experimental arrangement in the test section is shown in figure 2.

The water tunnel used is a closed-loop facility having a contraction ratio of 16. The test-section velocity and pressure can be controlled independently. In addition, the facility is equipped with a horizontal resorber consisting of a large tank of diameter 3.66 m and length 7.62 m in the lower leg just downstream of the main impeller. This ensures dissolution of the small air bubbles that are created in the test section owing to cavitation on the test bodies. Thus cavitation-noise measurements, which are essentially free from effects caused by the presence of air bubbles in the medium, can be performed at the inlet of the test section.

2.2. *Artificial nuclei by electrolysis*

The nuclei were artificially generated on the surface of the body by electrolysis. They were produced from a stainless-steel ring buried flush in the stagnation region of a non-conducting model. A schematic sketch in figure 3 shows the mounting details of the electrolysis ring. After fabrication, the nose portion was carefully examined using an optical comparator at 10× magnification to ensure that the shape of the body

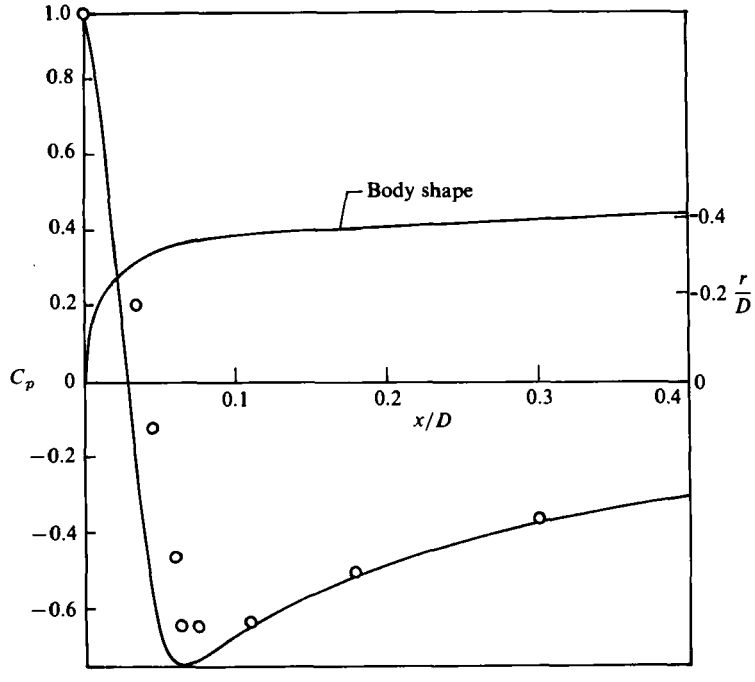

FIGURE 1. The test-body geometry, and the pressure distribution: ——, theoretical; O, measured.

was accurate (within about 20 μm) compared with that of the theoretical shape, and also to ensure that the ring did not protrude out of the boundary layer. The electrolysis bubbles were created by applying a d.c. voltage across the ring, which was used as one of the terminals, and the tunnel wall, which was the other. By making the ring the negative terminal, hydrogen bubbles were created at the ring and by reversing the polarity oxygen bubbles were created there.

The location of the ring was selected on the basis of an analysis which predicted the approximate diameter of the bubble at detachment at the typical test velocities. The details of the analysis are provided in Shanmuganathan (1984) but it should be noted here that the present location of the electrolysis ring at the mean radius of 12.5 mm was selected so that the size of nuclei leaving the ring would be around 50–100 μm over the speed range of the experiments. From static-stability analysis it is expected that cavitation from nuclei of this size range would be initiated as soon as the pressure falls slightly below vapour pressure. In addition to the above analysis, the sizes of the artificial nuclei were estimated with the help of a laser light-scattering device. These studies indicated that the dominant size of electrolysis bubbles was of the order of 50 μm. Owing to limitations in the instrumentation available it was not possible to exploit further this technique to obtain the number density of nuclei. However, qualitatively it was clear from the storage-oscilloscope traces (see Shanmuganathan 1984) that electrolysis was successful in injecting larger-sized nuclei in the boundary layer as compared with those existing naturally, and that the number density of nuclei could be altered by changing the electrolysis voltage. Even though the nucleus number density could be effectively controlled by changing the electrolysis voltage and also polarity there might always be a doubt whether the gas content of

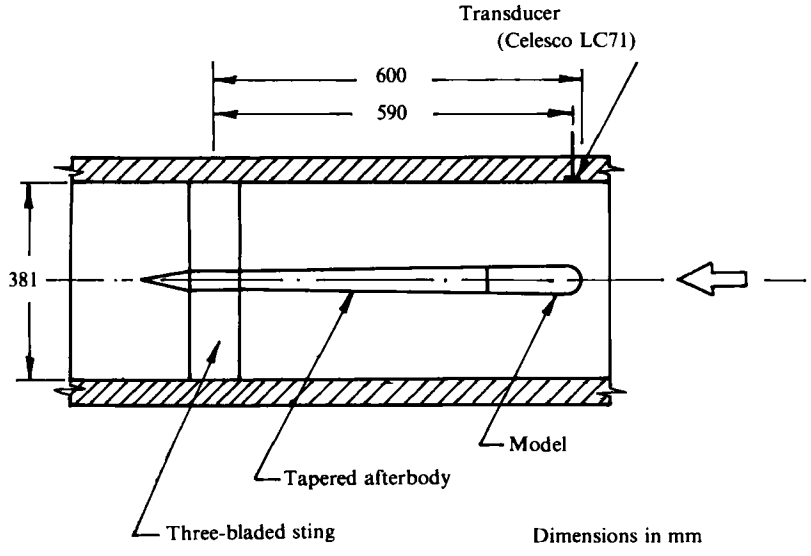

FIGURE 2. Schematic sketch showing the experimental arrangement.

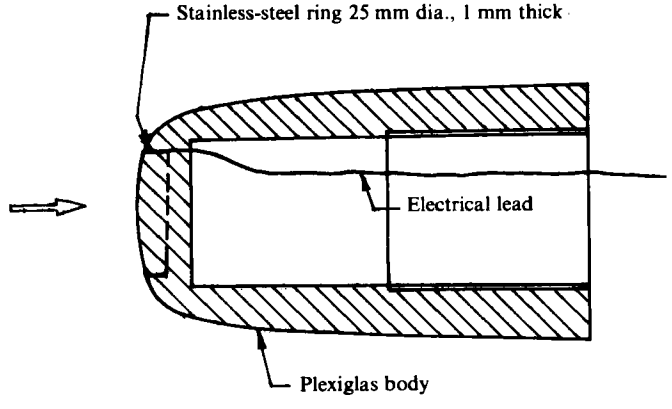

FIGURE 3. Schematic sketch showing the mounting details of the electrolysis ring.

the nuclei is also altered during this process. In view of this it was thought desirable to control the number density of nuclei by some independent means. With the present technique this was possible: the continuous-ring electrode was replaced on a separate model by twelve stainless-steel electrodes of 1 mm diameter placed at equal intervals at a mean diameter of 25 mm. Now, on application of electrolysis voltage, the nuclei would be generated from the isolated electrodes and would eventually, to a limited extent, become dispersed in the boundary layer downstream. Thus in this case the control on the number density of nuclei was possible owing to actual physical separation of the source of artificial nuclei.

2.3. *Noise-measurement equipment*

The sound-pressure levels were measured with a Celesco-71 piezoelectric transducer mounted flush in the test section as shown schematically in figure 2. The transducer has an active surface diameter of 5.28 mm, a charge sensitivity of 0.0286 PC/pascal and a resonant frequency of 150 kHz. The signal from the transducer was amplified

and conditioned using a B and K model 2650 precision conditioning amplifier in the charge mode. The amplified signal was recorded on a B and K model 2307 level recorder through a B and K model 2606 measuring amplifier and a B and K model 1617 third-octave filter. The signal could be directly recorded on a pre-calibrated chart by synchronizing the movement of the recorder paper and the scanning of the filter. With the above combination of instruments the averaging time is automatically controlled, depending on the centre frequency once the minimum value is set. In the present experiments the minimum value was set to be 1 s and it was found that this was sufficient since, owing to artificial seeding of nuclei, steady and regular cavitation was produced on the model. During preliminary experiments the minimum averaging time was increased to 10 s and virtually no difference was noticed in the spectra. It should be emphasized here that under natural conditions the cavitation events may not be so regular, in which case higher averaging times may be required. The complete system used for noise measurements was calibrated using a B and K model 4223 calibrator to confirm the charge sensitivity quoted by the manufacturer.

From the recorded signal the magnitude of the mean-square-sound-pressure levels, $\overline{p_s^2}(f, \Delta f)$ were obtained for different centre frequencies in the one-third-octave bandwidth. The sound pressure level L in decibels in this bandwidth is then defined as

$$L = 10 \log \frac{\overline{p_s^2}(f, \Delta f)}{p_0^2},$$

where p_0 is 1 μPa. For comparative studies it is convenient to correct L for the bandwidth and present the results in the spectral-density form, which is defined in decibels as

$$L - 10 \log \Delta f,$$

where Δf is the one-third-octave bandwidth at the frequency f. All noise measurements are presented here in the form of spectral densities *versus* frequency except when the results are non-dimensionalized. In the present work the emphasis is on comparative studies and hence the measurements are not corrected for any reverberation effects. It is expected that these effects, being due to geometry, would remain the same for all sets of measurements.

2.4. *Other general procedures*

The nominal water temperature for all studies was 25 °C and the air content was about 60 % saturation at atmospheric pressure. The static pressure in the test section was measured with a U-tube mercury manometer with one end open to the atmosphere. The velocity in the test section was computed from measuring the pressure drop across the contraction cone using another U-tube mercury manometer. The general procedure for noise measurements was first to fix a tunnel velocity and then gradually to reduce the tunnel static pressure to different levels and apply at each level several electrolysis voltages, namely 0, 9, 20, 40 and 60 V. This was repeated for different tunnel velocities and the entire operation was repeated for tests with reversed polarity and with the multielectrode body. Even though extensive data were obtained with these combinations, most of the results presented here are for electrolysis voltages of 9 and 20 V with hydrogen bubbles as nuclei, 20 V with oxygen bubbles and 9 V for the multielectrode body. In the following, unless specifically mentioned, the results refer to the continuous-ring-electrode model and hydrogen bubbles as nuclei. Following all noise measurements the continuous-electrode model was used for pressure-distribution measurements and the results are shown in figure 1.

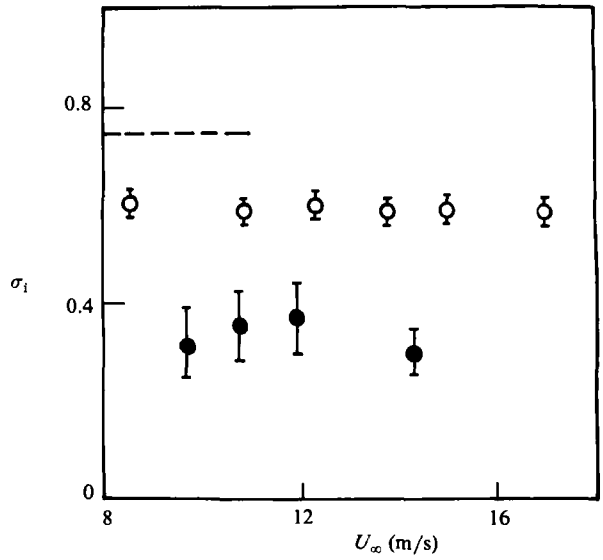

FIGURE 4. Cavitation-inception data: ●, without electrolysis (average of 4 readings at each velocity is indicated with bars showing the range of data); ○, with electrolysis, $E = 9$ V (average of 12 readings at each velocity is indicated with bars showing the range of data); – – –, theoretical value of $-C_{p\min}$.

3. Cavitation inception

Inception of cavitation was detected visually using stroboscopic lighting, both with and without electrolysis. The cavitation number σ is defined as

$$\frac{P_\infty - P_v}{\frac{1}{2}\rho U_\infty^2},$$

where P_∞ and U_∞ are the test-section static pressure and velocity respectively, ρ is the liquid density and P_v is the vapour pressure at the bulk temperature. The cavitation number at inception, designated by σ_i, is shown in figure 4 as a function of velocity for natural conditions and with electrolysis. Under natural conditions (i.e. without electrolysis) cavitation at inception was typically of the travelling-bubble type at lower velocities, but it changed to unsteady patch or attached patch for velocities exceeding 14 m/s; whereas with electrolysis it was always the travelling-bubble type at all the test velocities. Photographs of the natural cavitation could be obtained only at low σ-values when the cavity would remain attached to the model, and this is shown in figure 5(*a*). At essentially the same free-stream conditions the type of cavitation with electrolysis is shown in figure 5(*b*). The difference in the type of cavitation is evident.

From figure 4 it is apparent that the inception cavitation numbers without electrolysis are significantly lower than those with electrolysis. In particular, the difference between σ_i and $-C_{p\,\min}$ is of the order of 0.15 with electrolysis whereas it is of the order of 0.375 without. In addition, the magnitude of σ_i with electrolysis is found to remain nearly constant with increase in velocity, which is an important achievement considering the fact that natural σ_i depends on velocity in a complex manner. The influence of electrolysis voltage on σ_i was found to be small, with the σ_i value increasing from about 0.60 to 0.65 and an increase in electrolysis voltage from 9 to 60 V. On the other hand, with oxygen bubbles as nuclei, generated by reversing polarity, σ_i was somewhat lower, being of the order of 0.55.

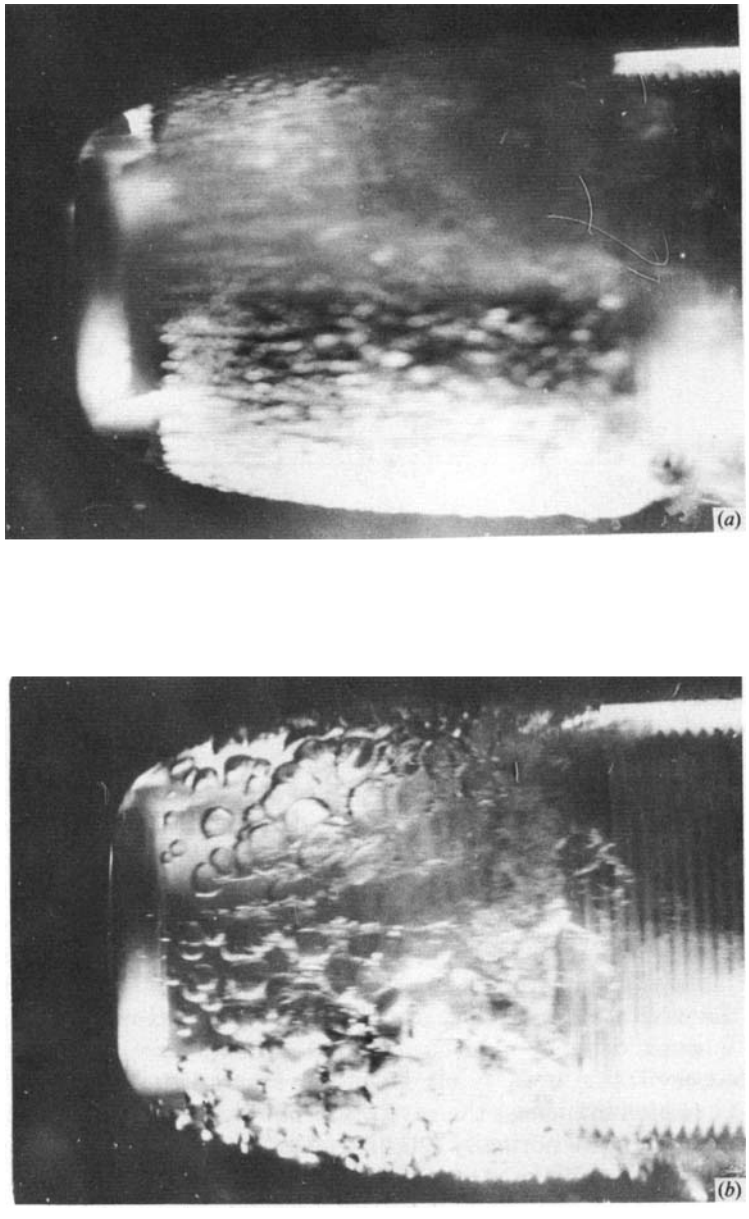

FIGURE 5. Photographs of cavitation with and without electrolysis. (*a*) Without electrolysis; $U_\infty = 10.8$ m/s, $\sigma = 0.32$. (*b*) With electrolysis; $U_\infty = 10.8$ m/s, $\sigma = 0.36$. The flow is from left to right.

4. Influence of various parameters on cavitation noise

4.1. *Electrolysis voltage*

The effect of electrolysis voltage on cavitation noise is shown in figure 6. With $E = 0$ V, at the conditions indicated, there is no cavitation on the model and the noise levels are primarily due to the small amount of cavitation on the supporting sting blades. However, with $E = 20$ V there is a substantial increase in the noise level over the entire frequency range and at higher frequencies than 10 kHz the difference exceeds 20 dB. With an increase in voltage to 40 and 60 V there is a gradual fall in

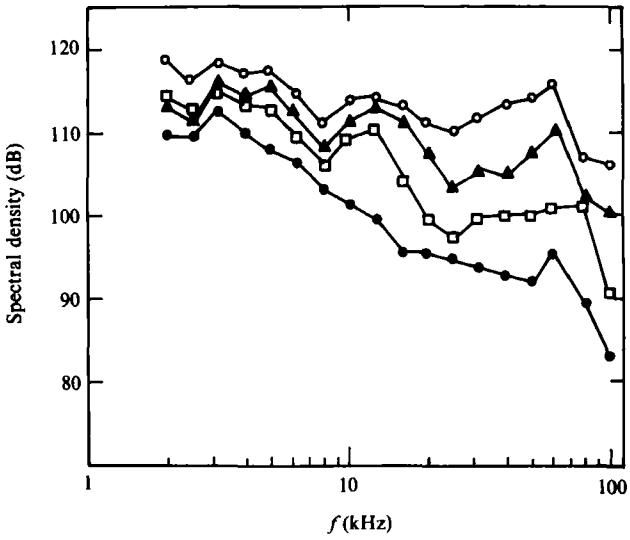

FIGURE 6. Spectral densities for $U_\infty = 10.0$ m/s, $\sigma = 0.56$: ●, $E = 0$ V; ○, 20 V; ▲, 40 V; □, 60 V.

the noise levels over the entire frequency range, the effect being more pronounced at higher frequencies.

Photographs of cavitation at different electrolysis voltages are shown in figure 7. It is apparent from the photographs that the number density of cavitation bubbles increases with an increase in electrolysis voltage. This was expected from the laser light-scattering observations, which indicated that the number density of nuclei increased with an increase in electrolysis voltage. From the middle photograph it is observed that the shape and maximum size of the cavitation bubbles is approximately the same as that for the bubbles in the first photograph, which corresponds to a lower voltage. However, with $E = 60$ V there is a definite reduction in the maximum size of the bubble, as is apparent from the bottom photograph, and this may explain the reduction in the cavitation-noise levels with $E = 60$ volts. However, the reduction with $E = 40$ V must depend on other reasons. In any case it has been clearly established that cavitation-noise levels depend on a parameter, namely the nucleus-number density (which influences the cavitation-bubble-number density in a cavitation zone) additional to the normally established parameters like cavitation number and free-stream velocity (Blake *et al.* 1977).

4.2. *Cavitation number*

The effect of cavitation number on the level of cavitation noise is shown in figure 8. As σ decreases the noise level is first observed to increase; however, below a certain σ-value, further decrease in σ results in the reduction of noise level over most of the frequency range. At σ-values lower than 0.4 the noise levels were almost equal to the background levels and hence are not included in figure 8. Cavitation photographs at different σ-values are shown in figure 9. Maximum cavitation-noise levels are observed to occur for the conditions similar to those shown in the top photograph, namely for $\sigma = 0.52$. Even though there is a substantial increase in the maximum bubble size as σ is reduced to 0.43 (as seen from the middle photograph), there is no corresponding increase in the cavitation-noise levels, as expected from single-bubble-dynamics

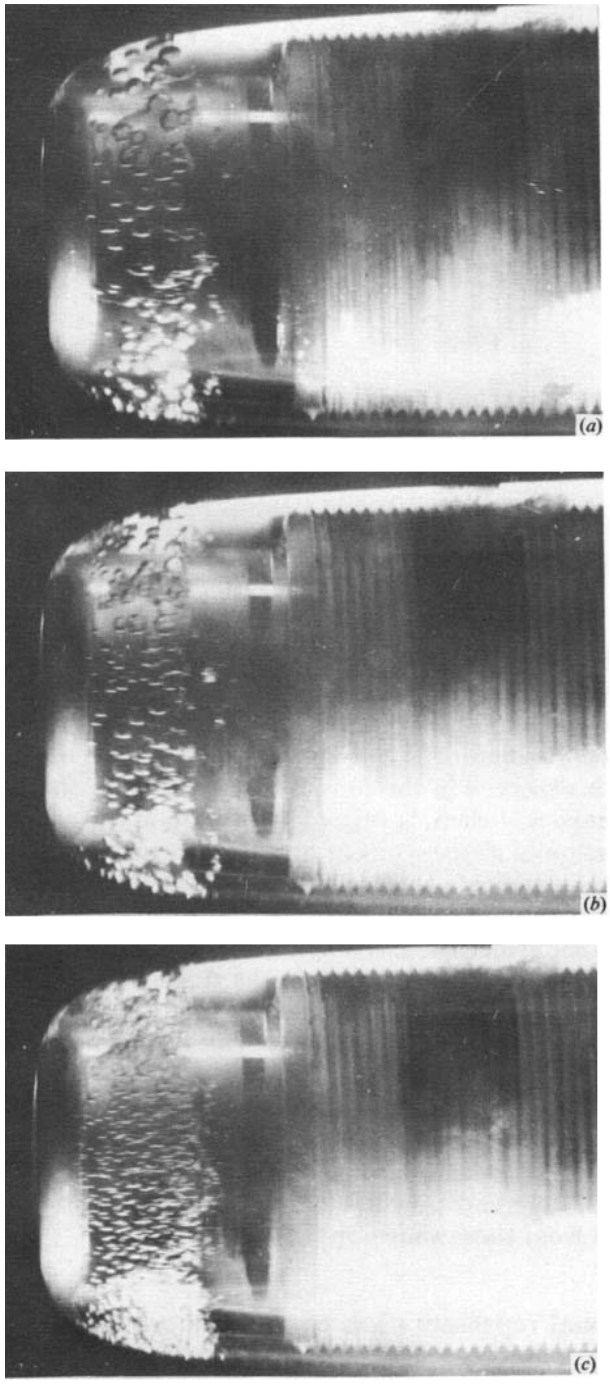

FIGURE 7. Photographs of cavitation with different electrolysis voltages for $U_\infty = 10.8$ m/s, $\sigma = 0.52$: (*a*) $E = 20$ V; (*b*) 40 V; (*c*) 60 V.

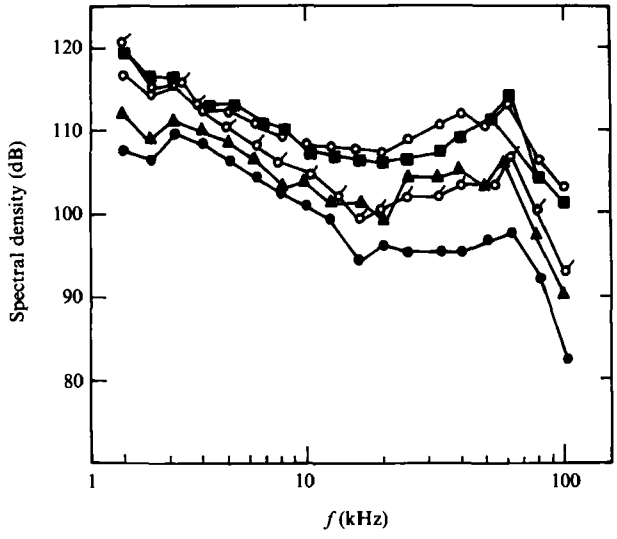

FIGURE 8. Spectral densities for $U_\infty = 10.8$ m/s, $E = 9$ V: ●, $\sigma = 0.60$; ▲, 0.57; ○, 0.52; ■, 0.48; ♂, 0.45.

theories (Fitzpatrick & Strasberg 1956) and experiments (Harrison 1952). On the contrary, the levels decrease, and this may be due to the fact that with the increase in bubble size there is almost a physical overlap of the bubbles. In addition there appears to be a definite distortion in bubble shape near the maximum radii. This is contrary to what is observed in the top photograph, where the bubbles are more or less spherical in shape and there is very little overlap of the cavitation bubbles. The overlap and distortion in shape worsens at $\sigma = 0.36$, as is evident from the bottom photograph, and, as indicated, at these σ values the noise levels have fallen substantially, being of the same order as background levels. The trends indicated were generally true at other velocities, electrolysis voltages and also for the multielectrode model. However, with oxygen bubbles as nuclei the noise levels increased monotonically as σ decreased, even to as low a value as 0.39. This point will be elaborated in §7.

4.3. *Velocity*

The effect of velocity on the cavitation-noise level is shown in figure 10. With increase in velocity there is a monotonic sharp increase in the noise levels for the range of velocities used here. This was also found to be the case for all other test conditions; however, the actual differences in the noise levels with increase in velocity differed to a certain extent from those shown in figure 10.

5. Non-dimensional representation of cavitation noise

The non-dimensional representation of cavitation noise is similar to that used by Blake *et al.* (1977). For this purpose two parameters are required, namely the maximum bubble radius R_m and the collapse time τ_0. These were estimated from the following relationships, which are also used by Blake *et al.*:

$$R_m = [\tfrac{1}{2}U_\infty^2(-\sigma - C_{pmin})]^{\frac{1}{2}}t', \tag{1}$$

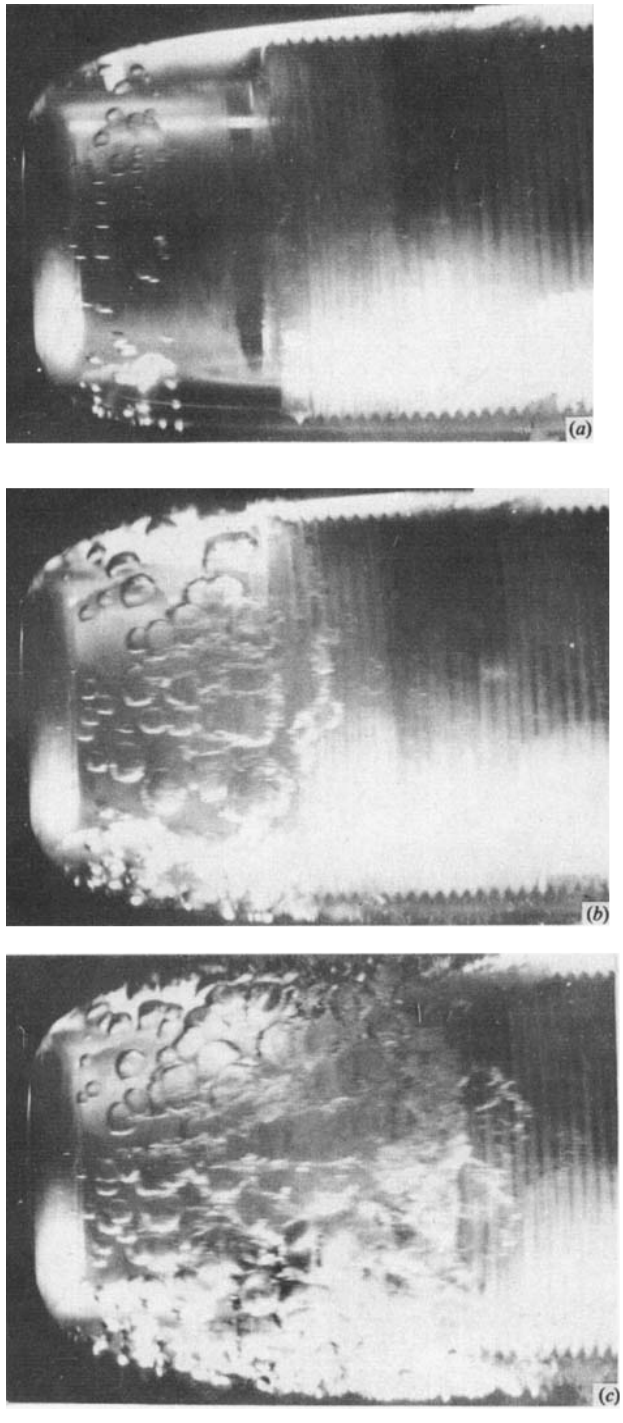

FIGURE 9. Photographs of cavitation with different cavitation numbers for $U_\infty = 10.8$ m/s, $E = 9$ V: (*a*) $\sigma = 0.52$; (*b*) 0.43; (*c*) 0.36.

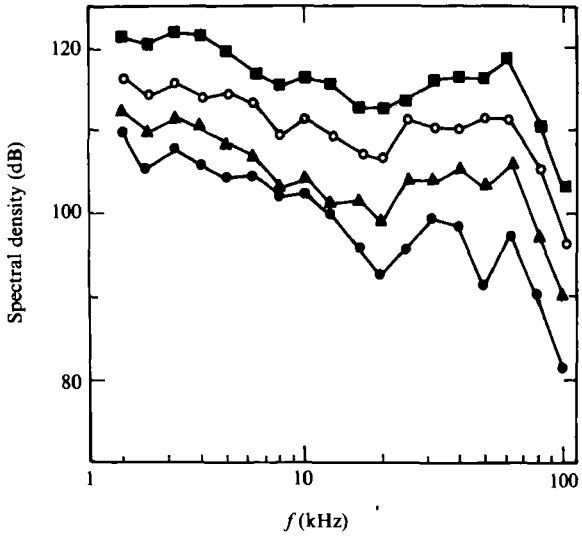

FIGURE 10. Spectral densities for $\sigma = 0.57$, $E = 9$ V: ●, $U_\infty = 8.6$ m/s; ▲, 10.8 m/s, ○, 13.6 m/s; ■, 17.0 m/s.

where t' is the length of time spent by the bubble in the region in which static pressure is less than vapour pressure or $p < p_v$. Here time t' is calculated from

$$t' = \left(\frac{l}{U_\infty}\right)(1-\bar{C}_p)^{\frac{1}{2}}, \tag{2}$$

where l is the chordwise extent of the region in which $p < p_v$ and $\bar{C}_p$ is the space-averaged static-pressure coefficient there. In the present case, l and $\bar{C}_p$ at a given σ were calculated from the theoretical-pressure-distribution curve. The collapse time is calculated from

$$\tau_0 = 0.915 R_m \left[\frac{\rho}{(P_\infty - P_v)}\right]^{\frac{1}{2}} = 0.915 \frac{R_m}{U_\infty}\left(\frac{2}{\sigma}\right)^{\frac{1}{2}}. \tag{3}$$

The estimated values from above were compared with the solution to the bubble-dynamics equation and were found to be accurate to within 15%. Similar agreement with measured values has been reported by Blake *et al.*

Using the parameters R_m and τ_0, the noise of a single spherical cavitation bubble has been shown by Fitzpatrick & Strasberg (1956) to have a frequency spectral density, $S_b(f)$, which is normalized as

$$\frac{S_b(f)\, r^2}{R_m^4 \rho P_\infty} = S_b(f\tau_0). \tag{4}$$

Here r is the acoustic range of the noise and the spectrum is defined such that

$$\int_0^\infty S_b(f)\, df = \int_0^\infty p_b^2(t)\, dt = \gamma\tau_0 \overline{p_b^2},$$

where $\gamma\tau_0$ is the total lifetime of the bubble expressed in multiples of τ_0. In the above, $p_b(t)$ is the sound-pressure level from the single-bubble motion and $\overline{p_b^2}$ is its

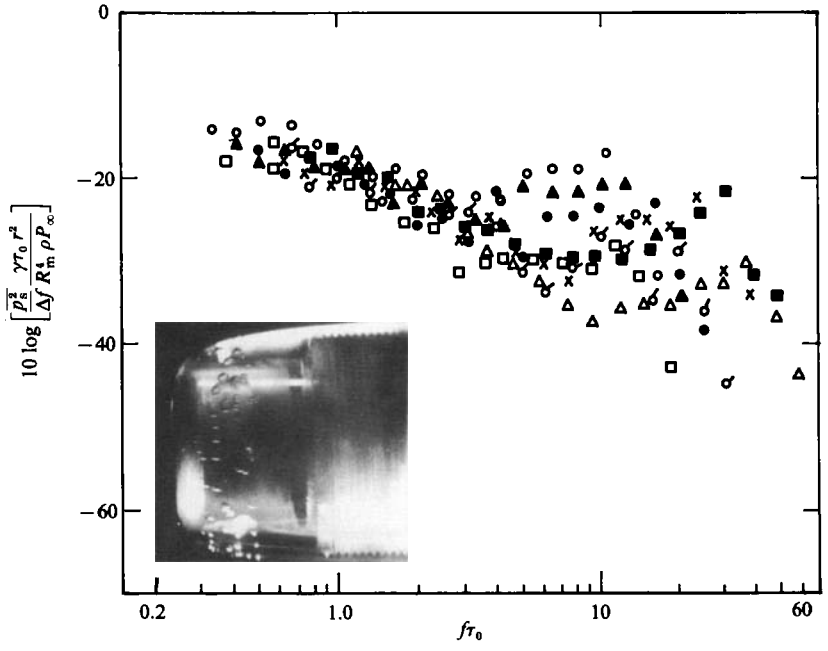

FIGURE 11. Non-dimensional spectral densities with hydrogen-bubble nuclei for $E = 9$ V.

$U_\infty = 8.6$ m/s	$U_\infty = 10.8$ m/s	$U_\infty = 13.6$ m/s	$U_\infty = 17.0$ m/s
○, $\sigma = 0.57$	□, $\sigma = 0.60$	▲, $\sigma = 0.57$	○, $\sigma = 0.57$
	● 0.57	× 0.51	
	■ 0.48		
	△ 0.45		

The conditions for the inset photograph are: $U_\infty = 10.8$ m/s, $\sigma = 0.52$.

time-averaged mean square. Again following Blake *et al.*, a measured sound-pressure level in a narrow frequency band Δf can be interpreted as a similar spectrum

$$S(f) = \frac{\gamma\tau_0 \overline{p_s^2}(f, \Delta f)}{\Delta f}, \tag{5}$$

and the normalization analogous to (4) is given by

$$S(f\tau_0) = \frac{\overline{p_s^2}(f, \Delta f)}{\Delta f} \frac{\gamma\tau_0 r^2}{R_m^4 \rho P_\infty}. \tag{6}$$

Here $\overline{p_s^2}(f, \Delta f)$ is the measured mean-square pressure in the filter band. The value of γ is usually taken to be 3, and this was confirmed from bubble-dynamics calculations. The non-dimensional spectral densities obtained using the procedure outlined above for the cases of hydrogen-bubble nuclei and electrolysis voltages of 9 and 20 are shown in figures 11 and 12 respectively. Similar data for oxygen-bubble nuclei and the multielectrode model are shown in figures 13 and 14 respectively. In all the cases as large a range as possible for the magnitudes of σ and U_∞ are included.

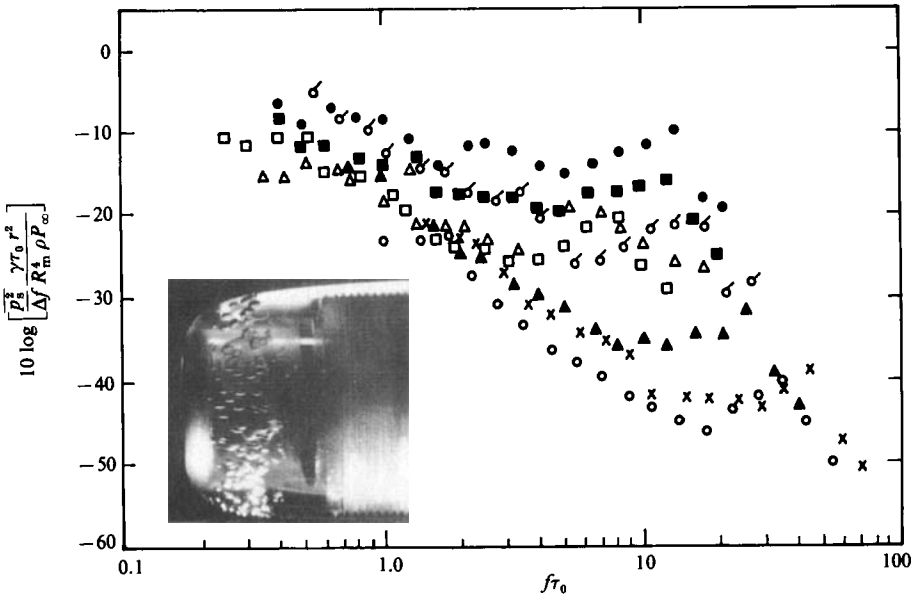

FIGURE 12. Non-dimensional spectral densities with hydrogen-bubble nuclei for $E = 20$V.

$U_\infty = 9.5$ m/s	$U_\infty = 11.5$ m/s	$U_\infty = 16.6$ m/s
●, $\sigma = 0.59$	△, $\sigma = 0.59$	□, $\sigma = 0.59$
▲ 0.52	♂ 0.55	■ 0.54
○ 0.48	× 0.41	

The conditions for the inset photograph are: $U_\infty = 10.8$ m/s, $\sigma = 0.52$.

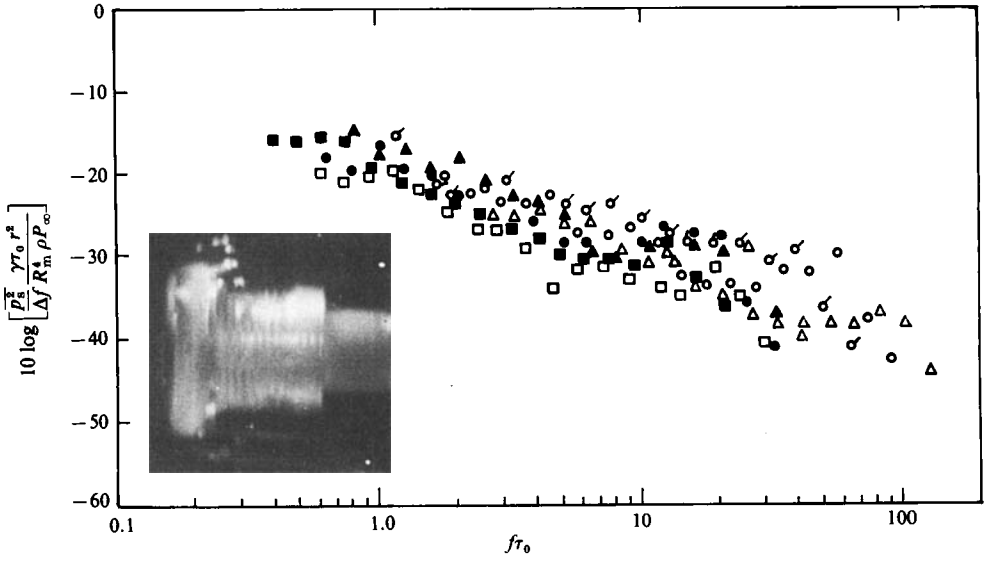

FIGURE 13. Non-dimensional spectral densities with oxygen-bubble nuclei for $E = 20$V.

$U_\infty = 8.6$ m/s	$U_\infty = 10.8$ m/s	$U_\infty = 16.6$ m/s
△, $\sigma = 0.35$	●, $\sigma = 0.53$	■, $\sigma = 0.54$
	▲ 0.50	□ 0.49
	♂ 0.44	
	○ 0.39	

The conditions for the inset photograph are: $U_\infty = 10.8$ m/s, $\sigma = 0.52$.

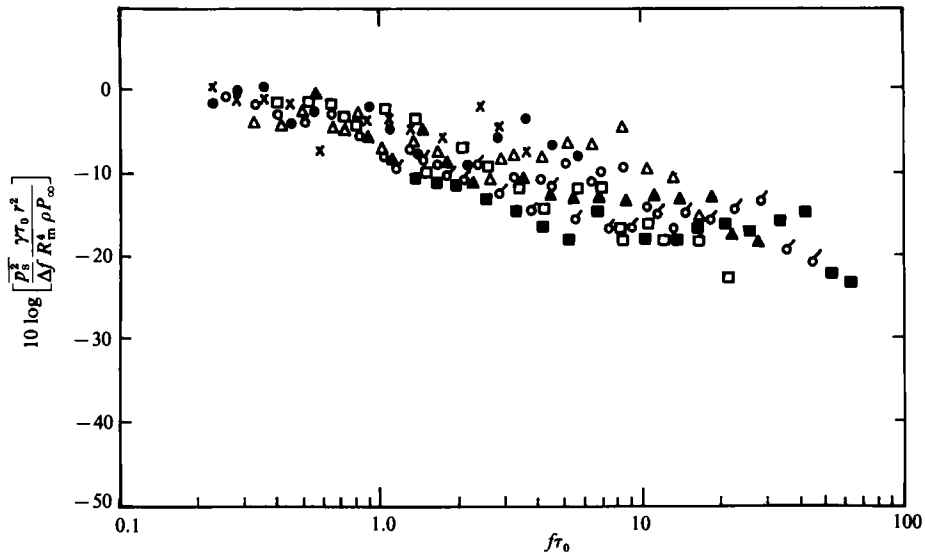

FIGURE 14. Non-dimensional spectral densities with multielectrode and hydrogen-bubble nuclei for $E = 9$ V.

$U_\infty = 8.6$ m/s	$U_\infty = 10.8$ m/s	$U_\infty = 13.6$ m/s	$U_\infty = 16.7$ m/s
△, $\sigma = 0.63$	●, $\sigma = 0.67$	○, $\sigma = 0.61$	×, $\sigma = 0.69$
○ 0.52	▲ 0.55	□ 0.56	
■ 0.47			

6. Evidence for interference effect

Results shown in figure 11 (hydrogen-bubble nuclei with 9 V) indicate that the collapse of data is quite good up to a value of $f\tau_0 = 3$. In particular it should be noted that the difference in the spectral-density value of about 20 dB for the cases of $U_\infty = 8.6$ m/s and $\sigma = 0.57$, and $U_\infty = 17.0$ m/s and $\sigma = 0.57$ in figure 10 is reduced to less than 5dB in figure 11 for these values of $f\tau_0$. However, for higher values of $f\tau_0$ there is a substantial scatter. Results in figure 12 (hydrogen-bubble nuclei with $E = 20$) show that the collapse is poor over almost the entire range of $f\tau_0$ values and there is only a semblance of collapse, if any, for values less than 1. Similar, in fact somewhat worse, behaviour was observed with electrolysis voltages of 40 and 60 V. In figure 13, with oxygen-bubble nuclei, the reverse trend is observed with a very good collapse of data over almost the entire $f\tau_0$ range. It is evident from the inset photographs of figures 11–13 that, given the same free-stream conditions, the number density of cavitation bubbles (which is a direct measure of number density of nuclei) increases almost twofold, with an increase in electrolysis voltage from 9 to 20 with hydrogen-bubble nuclei, and decreases substantially with oxygen-bubble nuclei. Therefore there is now systematic evidence that the observed behaviour of the non-dimensional spectral densities is related to an effect which may be termed an 'interference effect'. This effect could be taken to be a qualitative measure of the influence of neighbouring bubbles on the properties of cavitation noise relative to those expected on the basis of single-bubble behaviour. From the results presented in §4 we expect the interference effect to become significant either when a large nucleus-number density leads to the increase in the number of cavitation bubbles in a cavitation zone or when the cavitation number is reduced at a given nucleus-number

density, since this implies larger cavitation bubbles. In either case the net result is that the volume occupied by bubbles increases in the cavitation zone.

At this stage one may wonder whether the gas content of the bubbles, which is likely to vary with electrolysis voltage and polarity, is responsible for the observations, especially since the analysis of Fitzpatrick & Strasberg (1956) clearly shows that the presence of permanent gas in the bubble can result in multiple collapse and rebound cycles, thus significantly affecting the spectral distribution of cavitation noise. This point was investigated by the use of the separate model with a multielectrode. Hydrogen bubbles were the source of nuclei and an electrolysis voltage of 9 V was used. It may be recalled here that the surface area of the continuous-ring electrode was about eight times that of the combined surface area of the multielectrodes. The normalized cavitation-noise data for the multielectrode model are shown in figure 14. It is of interest to compare these with the results for the continuous-electrode model and with the same electrolysis voltage, shown in figure 11. It is clear that the collapse of data is significantly better over a wider $f\tau_0$ range for the multielectrode model. One may argue that the improvement observed in the collapse of data may be related to the possible effect of electrode configuration on bubble-size spectrum distribution. In particular, one could think of a narrower bubble-size spectrum in the multielectrode case as compared with that for the continuous one. However, even if this is a possibility, its effect on cavitation noise is not likely to be significant, since Flynn (1964) has shown that for a given sinusoidal pressure field the maximum radius to which a cavitation bubble will grow is relatively insensitive to initial radius provided it is larger than the critical radius required for cavitation initiation. Therefore we may now be reasonably convinced that the observed behaviour of the non-dimensional spectral densities is in fact primarily related to the bubble-interference effect.

7. Discussion of results

For a quantitative discussion on the interference effect we introduce the bubble volume fraction α, which has a value between 0 and 1. Flow regimes depending on the range of α may now be defined as in table 1.

The numerical values of α indicated in the above table are based on an estimation of the value of the void fraction from the top photographs of figure 7, 9 and the inset photograph of figure 13. First, the cavitation-bubble-number density was estimated by counting the number of bubbles in each of the photographs over a certain area of model; the respective approximate value being $11/\text{cm}^2$, $5/\text{cm}^2$, $2/\text{cm}^2$. Then the volume of each bubble was taken to be that corresponding to its maximum diameter. The volume of the liquid was taken to be the product of the area described above and its thickness, which was taken to be the maximum diameter of the bubble. It should be emphasized here that the void-fraction values obtained thus are very approximate and should be used only as order-of-magnitude estimates. Since α is a measure of the void fraction in a cavitation zone, we expect it to depend mainly on two factors: the number density of nuclei and the cavitation number.

From the above discussion we can infer that the interference is weak for the case of oxygen-bubble nuclei and the multielectrode model (figure 13 and 14); moderate for hydrogen-bubble nuclei with electrolysis voltage of 9 V (figure 11); and strong for hydrogen-bubble nuclei with 20 volts (figure 12) and greater. For the case of moderate interference we note that the scatter in the non-dimensional spectral-density plot is limited to high $f\tau_0$-values. In particular, the scatter appears to be related to the occurrence of a peak in the spectra at about 63 kHz, and the comparison

Range of α	Extent of interference	Implications for cavitation noise
0–0.1 (low)	Weak	Single-bubble-dynamics parameters can be used usefully to normalize cavitation-noise data over a wide $f\tau_0$-range
0.1–0.25 (medium)	Moderate	Single-bubble-dynamics parameters can be used usefully to normalize cavitation-noise data over a limited $f\tau_0$-range
0.25–1.0 (high)	Strong	Single-bubble-dynamics parameters cannot be used usefully to normalize cavitation-noise data over any $f\tau_0$-range

TABLE 1. Extent of interference and its implications

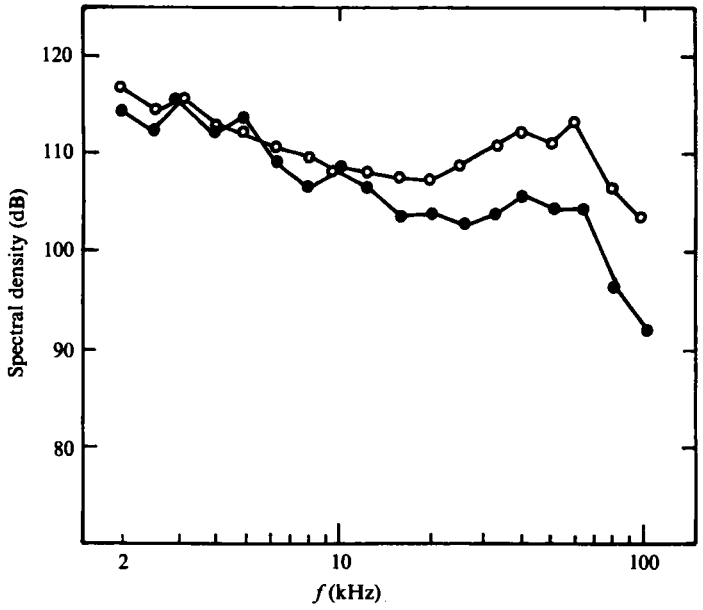

FIGURE 15. Influence of increased nucleus-number density on spectral-density–frequency dependence for $U_\infty = 10.8$ m/s, $\sigma = 0.52$–0.53; ○, hydrogen bubble ($E = 9$ V); ●, oxygen bubble ($E = 20$ V).

of the spectra for the two cases in figure 15 shows that the peak is distinct when nucleus-number density increases. For the case of strong interference we note that the scatter in the non-dimensional spectral-density plot can be related to the departure of cavitation-noise dependence on σ from that expected from single-bubble-dynamics behaviour, as is evident from the results presented in figure 16. For the oxygen-bubble nuclei case the spectral density continues to increase with reduction in σ, which is the expected behaviour as indicated earlier from the experimental observations of

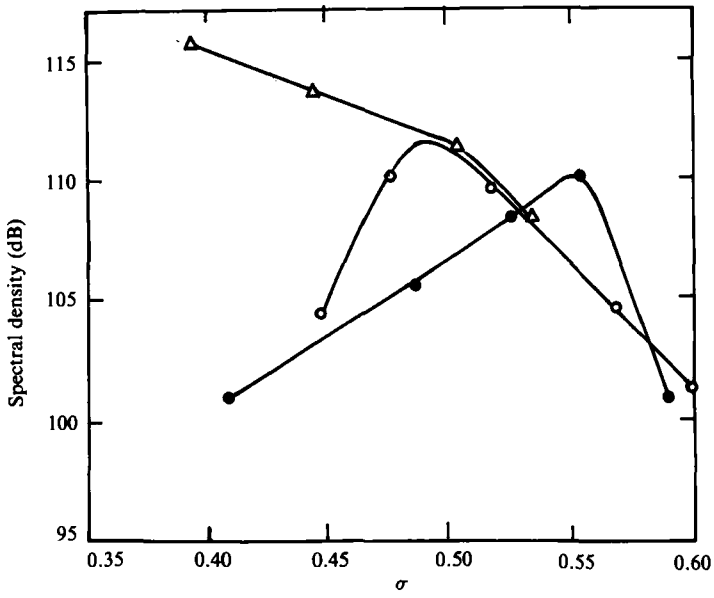

FIGURE 16. Influence of increased nucleus-number density on spectral-density–cavitation-number dependence for $U_\infty = 10.8$ m/s, $f = 10$ kHz: ●, hydrogen bubble ($E = 20$ V); ○, hydrogen bubble ($E = 9$ V); △, oxygen bubble ($E = 20$ V).

Harrison (1952) for single-bubble-cavitation noise and also from the theoretical work of Fitzpatrick & Strasberg (1956). However, with hydrogen-bubble nuclei and electrolysis voltage of 9 there is a departure from the expected behaviour at σ of about 0.49. This departure does not reflect strongly in the non-dimensional spectral-density plot of figure 11, since the σ-values are mostly above 0.49 and the spectral density is influenced by a peak at 63 kHz as mentioned earlier. With hydrogen-bubble nuclei and an electrolysis voltage of 20 the departure from the expected behaviour begins at σ of 0.56, which is as high as 93 % of inception σ-value. Therefore, the departure now reflects strongly in the non-dimensional spectral-density plot of figure 12, since now most of the σ-values are below 0.56. Under these conditions it is not surprising that the collapse of data based on single-bubble-dynamics parameters is extremely poor.

8. Summary

Cavitation-noise measurements from cavitation on an axisymmetric body are reported. Under various free-stream conditions a well-defined type of cavitation, namely the travelling-bubble type, was produced by injecting artificial nuclei generated by electrolysis in the boundary layer. The nucleus-number density was altered by changing the electrolysis voltage, polarity and geometry of the electrode. The change in cavitation-bubble-number density with alteration of nucleus-number density has been studied photographically.

Results normalized on the basis of single-bubble-dynamics parameters show clear evidence of an interference effect in cavitation noise. This effect seems to become prominent when the nucleus-number density is increased and at low cavitation numbers when maximum bubble radii are large. These observations suggest that the interference effect can be attributed to the effect of neighbouring bubbles on the

dynamics of individual cavitation bubbles. Qualitatively, the interference effect has been broadly classified as weak, moderate or strong, and to quantify this effect a factor equivalent to the void fraction has been used. When interference is weak the collapse of cavitation-noise data, obtained under various free-stream conditions and normalized on the basis of single-bubble-dynamics parameters, is good over a wide non-dimensional-frequency range. When interference is moderate, the collapse is good only up to a limited value of non-dimensional frequency. The scatter at the higher non-dimensional-frequency values is traced to the occurence of a peak in the spectra at about 63 kHz. When interference is strong, the collapse is poor over the entire non-dimensional-frequency range. This is traced to the departure of the dependence of spectral density with cavitation number from what is expected from observations of single-bubble-cavitation noise and from single-bubble-dynamics theory. This departure when the interference is strong can occur at σ-values which are as high as 93 % of the inception value. Under these circumstances, parameters based on treating the cavitation zone as a two-phase region may be more relevant for normalization rather than those based on single-bubble-dynamics approximations.

It is commonly observed that cavitation noise and damage intensity is reduced substantially by injection of air in the cavitation zone, the conventional explanation being that increased air content cushions the severe collapse of cavitation bubbles. However, the present work suggests that the interference effects owing to the increased nucleus-number density with air injection may be relevant to these observations.

The work reported here has formed part of the Ph.D. thesis of one of the authors (V. Shanmuganathan). The financial support has been partly provided by the Department of Electronics, Government of India, which is thankfully acknowledged. The staff of the Water Tunnel Laboratory is also to be thanked for their assistance in conducting the experimental studies. The authors would like to thank Mr Narayana Iyer for useful discussions and for obtaining one of the cavitation photographs used here. The authors are also grateful to Prof. G. K. Batchelor who, during his brief stay at the Indian Institute of Science, found time to make critical remarks on the original manuscript.

REFERENCES

ARAKERI, V. H. & ACOSTA, A. J. 1973 Viscous effects in the inception of cavitation on axisymmetric bodies. *Trans. ASME* I: *J. Fluids Engng* **95**, 519.

BLAKE, W. K., WOLPERT, M. J. & GEIB, F. E. 1977 Cavitation noise and inception as influenced by boundary layer development on a hydrofoil. *J. Fluid Mech.* **80**, 617.

FITZPATRICK, H. & STRASBERG, M. 1956 Hydrodynamic sources of sound. *2nd Symp. Naval Hydrodynamics, Washington, D.C.* 241.

FLYNN, H. G. 1964 Physics of acoustic cavitation in liquids. In *Physical Acoustics* (ed. W. P. Mason), vol. 1 (Part B), p. 57. Academic.

GATES, E. M. 1977 The influence of free stream turbulence, free stream nuclei populations and a drag-reducing polymer on cavitation inception on two axisymmetric bodies. Ph.D. thesis, California Institute of Technology, Pasadena.

GATES, E. M., BILLET, M. L., KATZ, J., OOI, K. K., HOLL, J. W. & ACOSTA, A. J. 1979 Cavitation inception and nuclei distribution. Joint ARL/CIT experiments. *Calif. Inst. of Tech. Rep.* no. E244.1.

HARRISON, M. 1952 An experimental study of single bubble cavitation noise. *D.T.M.B. Rep.* no. 815. DTNSRDC, Washington, D.C.

KELLER, A. P. 1972 The influence of the cavitation nucleus spectrum on cavitation inception, investigated with a scattered light counting method. *Trans. ASME* D: *J. Basic Engng* **94**, 917.

KNAPP, R. T. & HOLLANDER, A. 1948 Laboratory investigations of the mechanism of cavitation, *Trans. A.S.M.E.* **70**, 419.

PLESSET, M. S. 1949 The dynamics of cavitation bubbles. *Trans. ASME* E: *J. Appl. Mech.* **16**, 277.

RAYLEIGH (LORD) 1917 On the pressure developed in a liquid during the collapse of a spherical cavity. *Phil. Mag.* **34**, 94.

SCHIEBE, F. R. 1972 Measurements of the cavitation susceptibility of water using standard bodies. *St Anthony Fall Hyd. Lab. Rep.* no. 118. University of Minnesota.

SHANMUGANATHAN, V. 1984 Experimental studies on travelling bubble cavitation. Ph.D. Thesis, Indian Institute of Science, Bangalore.

VANDER MUELEN, J. H. J. 1976 A holographic study of cavitation on axisymmetric bodies and the influence of polymer additives. Ph.D. thesis, University of Twente, The Netherlands.